Materials Horizons

Voltage-tunable elastomer composites that use shape instabilities for rapid structural color changes

Journal:	*Materials Horizons*
Manuscript ID	MH-COM-03-2022-000374.R1
Article Type:	Communication
Date Submitted by the Author:	03-May-2022

Complete List of Authors:	Xiao, Ming; The University of Akron, Polymer Science Mao, Jie; Ningxia University, State Key Laboratory of High-efficiency Coal Utilization and Green Chemical Engineering Kollosche, Matthias; Harvard University, SEAS ; Hwang, Victoria; Harvard University, SEAS Clarke, David; Harvard University, School of Engineering and Applied Sciences Manoharan, Vinothan; Harvard University, Department of Physics

COMMUNICATION

Voltage-tunable elastomer composites that use shape instabilities for rapid structural color changes

Received 00th January 20xx,
Accepted 00th January 20xx

DOI: 10.1039/x0xx00000x

Ming Xiao,[a, b] Jie Mao,[a, c] Matthias Kollosche,[a] Victoria Hwang,[a] David R. Clarke,[a] Vinothan N. Manoharan[a,d,*]

Structurally colored materials can switch colors in response to external stimuli, which makes them potentially useful as colorimetric sensors, dynamic displays, and camouflage. However, their applications are limited by the angular dependence, slow response, and absence of synchronous control in time and space. In addition, out-of-plane deformation from shape instability easily occurs in photonic films, leading to inhomogeneous colors in photonic crystal materials. To address these challenges, we combine structurally colored photonic glasses and dielectric elastomer actuators. We use an external voltage signal to tune color changes quickly (much less than 0.1 s). The photonic glassses produce colors with low angular dependence, so that their colors are homogeneous even when they become curved due to voltage-triggered instabilities (buckling or wrinkling). As proof of concept, we present a pixelated display in which segments can be independently and rapidly turned on and off. This wide-angle, instability-tolerant, color-changing platform could be used in next-generation soft and curved color displays, camouflage with both shape and color changes, and multifunctional sensors.

New Concepts

The new concept we demonstrate is using shape instabilities to make a rapidly color-changing material. The material consists of colloidal particles embedded in a dielectric elastomer actuator. The particles are arranged such that they scatter light coherently, leading to structural colors. Previous work has shown that when the particles are ordered, forming a photonic crystal, their reflected colors can be tuned by applying an electric field to the elastomer. However, all such materials are subject to electric-field-triggered instabilities such as wrinkling and buckling. When these instabilities occur, the color of the embedded photonic crystal becomes inhomogeneous. Thus, the applied field is usually made small to avoid triggering the instabilities. We circumvent this problem by embedding a colloidal glass rather than a colloidal crystal in the elastomer. Because the glass is amorphous but retains short-range correlations, it produces a non-iridescent color that remains homogeneous even when the material buckles or wrinkles. This feature makes the system not only tolerant to instability, but also allows us to use instability to effect rapid, large color changes. These materials might be useful in flexible displays or responsive camouflage. More broadly, our work shows that instabilities can be harnessed in the design of responsive materials.

Introduction

Structural colors result from constructive interference of light scattered from nanoscale features rather than from absorption by molecules. Consequently, structurally colored materials can be made from many different component materials, such as natural polymers or responsive materials.[1,2] This versatility has enabled the fabrication of structurally colored materials that can change colors in response to external stimuli, such as humidity,[3] solvent,[3,4] light,[5–7] temperature,[8,9] mechanical force,[10–12] and magnetic,[13] and electric fields.[14] The wide range of tuning mechanisms makes structurally colored materials potentially useful for sensors, displays, camouflage, and anti-counterfeiting measures. But most of these applications require fast response and programmable control of color changes in both time and space. It is challenging to integrate these properties into one system, either because the component materials do not respond to the stimuli fast enough,[8,9,14] or because the stimuli cannot be controlled locally in a fast, precise, and programable way.[3,12,15,16]

[a.] *Harvard John A. Paulson School of Engineering and Applied Sciences, Harvard University, Cambridge MA 02138 USA, Email: vnm@seas.harvard.edu*
[b.] *College of Polymer Science and Engineering, Sichuan University, Chengdu, 610065, China*
[c.] *College of Chemical Engineering, Ningxia University, Yinchuan City, 750021, China*
[d.] *Department of Physics, Harvard University, Cambridge, MA 02138, USA*

Electronic Supplementary Information (ESI) available: [details of any supplementary information available should be included here]. See DOI: 10.1039/x0xx00000x

In principle, these challenges can be addressed by directly integrating structural colors into electroactive polymers used for dielectric elastomer actuators (DEAs), also known as artificial muscles.[17–19] DEAs are soft capacitors that allow for large but also fast voltage-controlled geometric deformation.[20–24] DEAs have been shown to allow direct tuning of structural color: mounted onto a DEA, a photonic crystal film follows voltage-induced strain of the DEA and changes colors.[25,26]

In practice, such bilayer designs using a photonic crystal film are subject to constraints due to the mechanical mismatch of the structurally colored film with DEAs and adhesion issues between the two layers. In addition, colors from photonic crystals are strongly angle-dependent, which is undesirable for many applications such as displays. Another limitation is the onset of electric-field-induced instabilities, such as buckling or wrinkling, which lead to nonuniform colors that are also unsuitable for many applications. To mitigate the onset of instabilities, large geometric pre-stretch can be applied, which is not compatible with all elastomers.[27]

Here we describe how to make responsive structurally colored materials that are not just tolerant to instabilities but can make use of them. To solve the problem of the color becoming inhomogeneous when instabilities arise, we use photonic glasses, which have isotropic, short-range correlations at scales comparable to visible wavelengths.[28–31] These materials can generate structural colors that vary little with either the viewing angle or sample orientation. By contrast, the structural color of a photonic *crystal* depends much more sensitively on the sample orientation than does a photonic glass. Because all shape instabilities create a gradient in surface normal, a photonic crystal under out-of-plane deformation produces many different reflected colors. By creating a composite of a photonic glass with a dielectric elastomer, we aim to produce homogeneous angle-independent colors when the material is subject to instabilities.

We embed the photonic glass directly into the dielectric film, thereby creating a material that responds rapidly to voltage-induced actuation. We prepare the photonic-glass composite by embedding a binary dispersion of silica nanoparticles into an elastic polymer network and stamping carbon nanotube (CNT) electrodes onto the composite film. We then directly apply a voltage across the film to generate a strain and consequently a change in color. As we shall show, we obtain homogeneous and angle-independent colors despite the curvature from out-of-plane deformation. As proof of concept, we present a pixelated display in which pixels can be rapidly turned on and off to show Arabic numerals from 0 to 9.

Results and Discussion

We make one set of DEA films containing photonic glasses and another set containing photonic crystals to characterize differences in how the optical properties change with an applied voltage. In both types of material, we embed 40% v/v silica nanoparticles in poly(ethylene glycol) phenyl ether acrylate (PEGPEA). The crystalline composite film contains monodisperse silica nanoparticles, while the glassy one contains a mixture of binary silica nanoparticles (see sample details in
Figure 1 caption and particle size distribution in Figure S1). The bimodal distribution from mixing two sizes of particles prevents crystallization, leading to a photonic glass, as also reported by Lee and co-workers.[32] We also add 0.15 $\pm$ 0.02% w/w carbon black with respect to the weight of silica nanoparticles to increase color saturation. We choose this carbon black concentration because it is sufficient to absorb most incoherent background scattering (Figure S2) but is well below the percolation threshold.[33] The materials show plastic deformation before 50% strain and their rupture strain reaches almost 100% (Figure S3). Both crystalline and glassy samples show large color changes and large elasticity as shown in Movie S1 and S2. From the elastic deformation region in the stress-strain curve, we calculate that elastomer composites have Young's modulus of 1588 $\pm$ 27 KPa.

Our photonic composites show continuous color changes under uniaxial stretching (Figure S4). The crystalline sample's reflectance peak shifts to shorter wavelengths by (18.0 $\pm$ 0.1)% under 40% strain under normal incidence and detection; and the glassy sample shifts by (16.0 $\pm$ 0.1)% under 40% strain. From uniaxial tensile tests for ten cycles with a maximum strain of 40% and a stretching speed of 1% strain per second, we find that the remaining strain is about 10% after the first cycle and the hysteresis becomes much lower over the last 9 cycles (Figure S5). This is likely because the first cycle releases the prestrain induced by polymerization in the fixed glass chambers.

The colors are reversible during the mechanical cycles, as seen in Movie S3. The demonstration of this mechano-chromic property relating strain to color suggests that we can change color by directly applying a voltage across the thickness direction of our composite films to create a compressive, electrostatic force on the film.

To demonstrate voltage-actuated color changes, we prepare rectangular strips of photonic elastomer films, and then use a stamp transfer process[34] to put CNT electrodes on both sides. The CNT electrode slightly decreases the reflectance (Figure S6). We mechanically constrain the film strip by attaching it to an acrylate frame without pre-stretching (
Figure 1A). Then, when we apply a voltage signal, the resulting electrostatic (Maxwell) pressure causes the thickness to decrease with a corresponding expansion of the electrode area of the film (
Figure 1B). At a critical electric field, the constrained expansion of the film leads to out-of-plane deformation through buckling or wrinkling. Under a sinusoidal electric field (frequency 0.33Hz, maximum amplitude 1.7 kV), we observe color changes and buckling for both crystalline and glassy films (Movie S4 and S5).

Whereas the color of the crystalline film varies across the electrode area when the material buckles (**Figure 1**C), the color of the glassy film is homogeneous across the electrode area (**Figure 1**D). To understand the origins of these different optical responses, we comprehensively quantify the color changes. The color of the crystalline composite shifts from red to green when the camera angle changes from 3° to 50° (see the measurement setup in Figure S7), while the color of the glassy sample changes much less (**Figure 2**A-B). Consistent with the visual appearances, the glassy sample has a smaller peak shift than the crystalline one when the incident angle varies from 10° to 30°: the glassy sample has a 34 nm blue shift from 580 nm to 546 nm and the crystalline sample has a 75 nm shift from 625 nm to 540 nm (**Figure 2**C-D). Using the CIELAB color standard (*23*), we calculate that the color difference is 42.3 for the crystalline and 5.8 for the glassy sample, showing that the color of the glassy sample is much less sensitive to angular variations. As shown in Figure S8-S9, the angular dependence decreases when the doping ratio of secondary particles increases from 0% to 40% (the doping ratio is the volume ratio of secondary particles, 164 nm, relative to the main particles, 204 nm). We choose a 20% doping ratio so that the angular dependence is weak and the color saturation is not too low.

To further quantify the angular dependence of photonic elastomer films, we perform angle-resolved scattering experiments in three different geometries (Figure S10). In the first measurement, the incident and detection angles are identical. We find that the crystalline sample has higher and sharper reflectance than the glassy sample, and both spectra shift to shorter wavelengths with increasing incident angles. In the second measurement, the incident light normal to the sample surface is held constant and the detector angle varies. We find that the glassy sample has much lower reflectance, and its spectra have smaller changes in peak position compared to the crystalline sample. In the third measurement, the angle between the light source and the detector is constant and the sample is tilted. We find that the reflectance spectrum of the crystalline sample changes markedly, while the spectrum of the glassy sample shows only minor changes in both intensity and peak position. Taken together, these measurements show that the color of the glassy sample varies much less strongly than the crystalline sample with respect to both the source-sample-detector angle and the sample orientation.

The differences in optical behavior of the crystalline and glassy samples originate from their nanostructural arrangement. The monodisperse silica nanoparticles in the crystalline sample form an ordered crystalline packing (**Figure 2**E) that diffracts light at specific angles, leading to high angular dependence. The bidisperse nanoparticles form an amorphous structure with short-range correlations (**Figure 2**F) that coherently scatters light, reducing angular dependence. When the electric field triggers out-of-plane deformation, resulting in a curved surface as shown in **Figure 1**C-D, the crystalline film reflects light of different colors, whereas the glassy one reflects homogeneous colors. We attribute this result to the low angular dependence of the glassy sample, which allows homogeneous colors even in the buckled state.

Although we can directly tune the colors of photonic elastomers using the electric field, two improvements help to avoid premature electrical breakdown. First, inspired by work from Chang and Park to maintain an electrode's conductivity under high strain,[25] we stamp transfer CNT electrodes (overlapping area is 10 mm × 10 mm) onto an uniaxially stretched elastomer (pre-stretch strain = 20%) and then release the strain to 10% before testing the films (Figure S11). The final electrode area is about 9 mm × 10 mm. Second, we pre-condition the films using a "proof test" to remove soft breakdown paths that can otherwise lead to premature electrical failure.[36] This pre-conditioning is performed by applying 10 cycles of a series of sinusoidal voltages (0.5 Hz from 1.0 kV to 2.0 kV with an increment of 0.2 kV).

We apply these treatments to glassy films and then quantify the voltage-actuated color and shape changes. Because the actuating voltage scales inversely with film thickness, large thicknesses would require higher driving voltages. To allow manual handling of the thin elastomer films and avoid electrical breakdown, we choose the film thickness to be 125 μm and limit the driving voltage to 3 kV.

The resulting materials show noticeable color changes from green to blue at 2 kV (**Figure 3**). As shown in Movie S6, the film shows reversible changes in color and shape at 3 kV and a frequency of 0.5 Hz. The reflectance spectrum shifts to shorter wavelengths when voltage increases (**Figure 3**B). To quantify the shape change, we use a laser scanner to measure the surface profile of wrinkled films when actuated under the voltage. From the surface profile, we extract the height profile of the electrode area along the *x* direction. We find that the height changes become larger above 2 kV (**Figure 3**C).

We use the sample's contour lengths to quantify out-of-plane deformation, since larger deformation leads to longer contour lengths. To correlate color changes with out-of-plane deformation, we plot the reflectance peak positions and the electrode's center contour lengths (arc lengths of curves in **Figure 3**C) as a function of the voltage. The reflectance peak shifts to shorter wavelengths and the arc length increases with the voltage. There are sharp changes in both the peak wavelengths and arc lengths when the voltage increases from 1.8 to 2.2 kV, where instability occurs. A surface profile of the film confirms that it has a wrinkling pattern at 2 kV (**Figure 3**D). This result suggests that we can utilize instabilities to trigger larger color changes.

We use this instability-triggered color changing system to make a dynamic pixelated display. We prepare seven separate pixels so that we can independently control each pixel to show an Arabic numeral. The pixels have a width of 2 mm, which is set by the size of the electrodes we can design and make. Smaller pixels could in principle be made using established methods to make electrodes for micrometer-scale circuits.

The device shows dark green at the electrode areas, and the pixels turn to blue when the voltage is applied. As shown in **Figure 4**A, the device shows number patterns from 0 to 9 under 2 kV. The dynamic color changes are more apparent in Movie S7, which shows the displayed digits changing in real time. All pixels undergo instabilities: some buckle and some wrinkle. Despite these different types of instability, the colors are homogeneously blue. In addition, the colors of the activated pixels change little when viewed from a different angle (Figure S12). These results further demonstrate the advantages of using photonic glasses as part of the responsive system.

We further investigate how the display changes colors under different frequencies of the sinusoidal voltage signal. For all four frequencies (0.5 Hz, 2 Hz, 5 Hz, and 10 Hz), cycling the voltage leads to the numeral 3 turning on and off, as desired (Movie S8). To quantify how the color changes with frequency, we extract the green channel values of the RGB-encoded frames of the recorded movies. As shown in **Figure 4**B, the color of the pixelated display reversibly changes with sinusoidal voltages from 0.5 Hz to 10 Hz. This suggests that the color switching time is much smaller than 0.1 s, which is faster than electrochromic materials based on chemical reactions (more than 1 s)[37,38] or structurally colored displays where particles are moving in solution under voltages (1–2 s).[14] In addition, the latter two systems need even longer times (up to several minutes) to switch back to their original colors. Thus, we can use the electric field to rapidly and precisely change colors in time and space.

Conclusions

We made an all-solid-state color-changing system by integrating structural color and dielectric elastomer actuation. We have shown that the electric field can be used to directly change colors, without any chemical reaction. More importantly, because our device uses a photonic glass, it is free of iridescence and shows homogeneous colors even when out-of-plane deformation generates curvature. This last effect is not possible for a photonic crystal, because a curved surface reflects different colors. In addition, a photonic glass is easier to formulate than a photonic crystal.

The use of photonic glasses allows us to take advantage of shape instabilities, rather than avoiding them. The colors remain homogeneous despite wrinkling or buckling. Color changes become more obvious after instabilities occur, indicating that we can obtain larger color changes when films undergo shape instabilities. Another useful feature of using instabilities to change colors is that this approach saves horizontal space and facilitates the design of pixelated and curved color displays.

As a proof of concept, we made a dynamic pixelated display that can change color in each pixel independently to show Arabic numerals with voltage. We demonstrated that the display can reversibly change colors at frequencies of 10 Hz. Our voltage-actuated system combines fast, temporal, spatial, and programable control of colors, which is not currently possible for light-driven,[7,39] temperature-driven,[8] mechanical,[10] or pneumatic color changing systems.[12]

In the future, we aim to make even faster and larger color changes for broader applications. To make faster color changes, we must minimize the hysteresis, which is determined largely by viscoelasticity. One possible approach is to increase the cross-linking density, especially the cross-linking between particles and the elastomer matrix. To make larger color changes, we must make a system that can attain a larger deformation before the breakdown voltage is reached. It may be possible to do this by replacing the rigid silica particles with softer and elastic colloidal particles. This change would not only enable larger color change but also decrease actuated voltages, making this new color-changing platform suitable for camouflage, sensors, or other applications, in addition to color displays.

Experimental Section

Safety and hazards. When making the elastomers, one needs to be aware that PEGPEA is classified as an irritant, and 2-hydroxy-2-methyl-1-phenyl-1-propanone is classified as an irritant and environmental hazard. Appropriate personal protective equipment should be used with all reagents, and materials should be handled in a fume hood. UV-absorbing shields should be used when irradiating materials with UV light. The high voltages used for actuation carry a risk of electric shock. This risk can be reduced by using a self-stop system that allows a maximum current to be set.

Preparation of photonic elastomers. We modified a reported protocol to a photonic elastomer composite.[10] We first prepared silica dispersions in an acrylate-based monomer solution. Silica nanoparticles (purchased from NanoCym) were washed with anhydrous ethanol three times before use. We then dispersed unary or binary mixtures of silica nanoparticles in anhydrous ethanol with a concentration of 10% w/w. The mixture is blended with a macromonomer, poly(ethylene glycol) phenyl ether acrylate (PEGPEA, MW 324, Sigma-Aldrich) containing 1% w/w of photoinitiator (2-hydroxy-2-methyl-1-phenyl-1-propanone, Sigma-Aldrich). This was then left overnight at 70°C for the ethanol to evaporate, leading to a self-assembled photonic liquid showing colors. The refractive indices of silica and PEGPEA are 1.458 and 1.502 at wavelength of 589 nm. We then infiltrated the photonic liquid into a chamber made of two glass slides with a 125 μm Kapton film as

a spacer. We annealed the photonic liquid in the glass chamber at 70°C for 4 hours and then put it in a UV chamber (UVP Crosslinker CL-1000, 254 nm, 8 W) for 5 min. After the liquid solidified, we removed the glass slide and peeled off the photonic elastomer. To ease subsequent peeling, we spin-coated a sacrificial layer of water-soluble dextran (MW 15000-25000, Sigma Aldrich) onto the glass slide.

Optical characterization. We used a Cary 7000 universal measurement spectrometer to quantify the angular dependence of photonic elastomers. The light source was a Neon lamp. To measure the integrated reflectance, we used an integrating sphere (Labsphere) accessory with a center mount. The sample was mounted on a black substrate, so all the scattered light to the detector represents the reflectance of the sample alone. The sample was illuminated with light from a double out-of-plane Littrow monochromator on a 1 mm × 3 mm rectangular spot. We rotated the sample angle so that the angle between the incident direction and the sample surface normal varied from 10 to 30°. We normalized the reflectance with a mirror at the center mount and with an incident angle of 30°. Then we used a goniometer accessory to measure the reflectance at different incident and detecting angles. The detector collected all the light within 5°, as set by the aperture.

Nanostructural characterization. We used a field emission scanning electron microscope (Zeiss Ultra Plus) to measure the silica particle sizes and nanostructures of photonic elastomers. The electron voltage was 3 kV. To take cross-sectional SEM images of the photonic elastomers, we cut them using a knife and sputter coated the cut face with Pt/Pd 80/20 alloy using a metal sputter coater (EMS 150T S).

Tensile Tests. We performed the tensile tests of glassy and crystalline elastomer films using a linear tensile tester (Instron 5544) equipped with a 10 N load cell. The films were cut with a laser cutting system to obtain strips with dimension 10 mm x 75 mm. The sample were clamped such that the active region had the dimensions of 10 mm x 50 mm. The samples were stretched with a constant strain rate of 1 %/s until rupture and the Young's modulus was extracted by linear fitting the first 50% stress-strain curve. We also ran cyclic stretching tests to investigate the hysteresis of elastomer films. The samples were periodically stretched with a constant strain rate of 1%/s between two different strain positions for ten cycles with a maximum strain of 40%.

Electrode fabrication. We follow a reported protocol to use CNT as a compliant electrode in our experiments.[34] The CNT electrodes were prepared from a commercially available CNT solution (Invision 1210, NanoC) and stamp-transferred onto both sides of the elastomer film. We diluted 50 μL CNT ink in 8 mL isopropanol directly before a vacuum filtration step through a porous polytetrafluorethylene (PTFE) filter membrane (0.2 μm pore and 47 mm diameter, Nuclepore®, Whatman, Florham Park, NJ, USA). The resulting CNT film on the PTFE filter membrane had a sheet resistance of 1200 Ohm/Sq (20J3 Sheet Resistance Meter, DELCOM Instruments, INC.). The CNT layer was stamp-transferred onto the elastomer surface through a mask to define the electrode area. Then the PTFE filter was peeled off from the elastomer surface. That procedure was repeated on the opposite side of the elastomer surface. Electric connections to electrodes were established using a carbon conductive tape.

Actuator device fabrication. The DEAs were prepared in two different ways. The first method used unstrained films (as shown in

Figure **1**). We mounted the photonic elastomer on to a laser-cut acrylic frame and applied a mylar mask onto the films that defines the electrode's geometry. We stamp transferred a carbon nanotube (CNT) film onto mask-covered photonic films. We then fixed the frame and connected the CNT electrodes using carbon-black conducting tape. In the second method, we pre-stretched and then released the film. Then, the elastomer film was mounted onto a laser-cut stretcher frame and then stretched uniaxially by 20% (Figure S11). After applying a Mylar mask and stamp transferring CNTs, we released the stretched film to 10% strain.

Actuation experiments with quantitative measurements. We applied the voltages across the thickness direction of photonic actuators to produce deformation and color changes. We controlled the voltage signal using a high-voltage power supply (Trek 610E, Trek Inc.) controlled by Labview. We put the sample in a light box and used a DSLR camera (Sony Alpha 7S II) to record the color changes. To quantify color changes when actuated, we collected reflectance spectra of the center positions of the actuators using an optical-fiber-connected spectrometer (Ocean Optics HR2000+) attached to a Nikon ECLIPSE LV100 microscope (10× objective, NA 0.3). To quantify the surface profile of actuators under deformed or buckled state, we used a laser scanner (MTI ProTrak PT-G 60-40-58) and a precision linear stage (GHC SLP35, GMC Hillstone Co. and MicroFlex e100 servo drive) to move the samples.

Author contribution

Conceptualization: MX, JM, VNM, DC. Investigation: MX, JM, MK, VH. Visualization: MX, VNM, JM, MK. Supervision: VNM, DC. Writing—original draft: MX, VNM. Writing—review & editing: all authors

Conflicts of interest

The authors declare that they have no competing interests.

Acknowledgements

We thank Ehsan Hajiesmaili for helpful discussion on voltage actuation experiments and Arthur McClelland for the help in some optical measurements. This work was supported in part by the Harvard MRSEC under National Science Foundation grants DMR-1420570 and DMR-2011754. It was performed in part at the Harvard Center for Nanoscale Systems, supported by NSF Grant 1541959.

References

1 Z. Zhang, Z. Chen, L. Shang and Y. Zhao, *Advanced Materials Technologies*, 2021, 2100296.
2 G. Isapour and M. Lattuada, *Advanced Materials*, 2018, **30**, 1707069.
3 M. Xiao, Y. Li, J. Zhao, Z. Wang, M. Gao, N. C. Gianneschi, A. Dhinojwala and M. D. Shawkey, *Chemistry of Materials*, 2016, **28**, 5516–5521.
4 M. Malekovic, M. Urann, U. Steiner, B. D. Wilts and M. Kolle, *Advanced Optical Materials*, 2020, **8**, 2000165.
5 Y. Wang, M. Li, J.-K. Chang, D. Aurelio, W. Li, B. J. Kim, J. H. Kim, M. Liscidini, J. A. Rogers and F. G. Omenetto, *Nature communications*, 2021, **12**, 1–9.
6 S. Li, Y. Zeng, W. Hou, W. Wan, J. Zhang, Y. Wang, X. Du and Z. Gu, *Materials Horizons*, 2020, **7**, 2944–2950.
7 Y. Wang, Z. Zhang, H. Chen, H. Zhang, H. Zhang and Y. Zhao, *Science Bulletin*, 2022, **67**, 512–519.
8 Y. Ohtsuka, T. Seki and Y. Takeoka, *Angewandte Chemie International Edition*, 2015, **54**, 15368–15373.
9 S. Y. Lee, J.-S. Lee and S.-H. Kim, *Advanced Materials*, 2019, **31**, 1901398.
10 G. H. Lee, T. M. Choi, B. Kim, S. H. Han, J. M. Lee and S.-H. Kim, *ACS Nano*, 2017, **11**, 11350–11357.
11 M. Kolle, A. Lethbridge, M. Kreysing, J. J. Baumberg, J. Aizenberg and P. Vukusic, *Advanced Materials*, 2013, **25**, 2239–2245.
12 S.-U. Kim, Y.-J. Lee, J. Liu, D. S. Kim, H. Wang and S. Yang, *Nature Materials*, 2021, **21**, 41–46.
13 Z. Li, M. Wang, X. Zhang, D. Wang, W. Xu and Y. Yin, *Nano Lett.*, 2019, **19**, 6673–6680.
14 A. C. Arsenault, D. P. Puzzo, I. Manners and G. A. Ozin, *Nature Photonics*, 2007, **1**, 468–472.
15 Y. Zhang, Y. Wang, H. Wang, Y. Yu, Q. Zhong and Y. Zhao, *Small*, 2019, **15**, 1902198.
16 Y. Yue, T. Kurokawa, M. A. Haque, T. Nakajima, T. Nonoyama, X. Li, I. Kajiwara and J. P. Gong, *Nature Communications*, 2014, **5**, 4659.
17 Y. Qiu, E. Zhang, R. Plamthottam and Q. Pei, *Accounts of Chemical Research*, 2019, **52**, 316–325.
18 Z. S. Davidson, H. Shahsavan, A. Aghakhani, Y. Guo, L. Hines, Y. Xia, S. Yang and M. Sitti, *Science Advances*, 2019, **5**, eaay0855.
19 C. Christianson, N. N. Goldberg, D. D. Deheyn, S. Cai and M. T. Tolley, *Science Robotics*, 2018, **3**, eaat1893.
20 R. Pelrine, R. Kornbluh, Q. Pei and J. Joseph, *Science*, 2000, **287**, 836–839.
21 A. Ryabchun, M. Kollosche, M. Wegener and O. Sakhno, *Advanced Materials*, 2016, **28**, 10217–10223.
22 X. Zhao and Z. Suo, *Physical Review Letters*, 2010, **104**, 178302.
23 Y. Chen, H. Zhao, J. Mao, P. Chirarattananon, E. F. Helbling, N. P. Hyun, D. R. Clarke and R. J. Wood, *Nature*, 2019, **575**, 324–329.
24 E. Hajiesmaili and D. R. Clarke, *Nature Communications*, 2019, **10**, 183.
25 H.-K. Chang and J. Park, *Advanced Optical Materials*, 2018, **6**, 1800792.
26 D. Y. Kim, S. Choi, H. Cho and J.-Y. Sun, *Advanced Materials*, 2019, **31**, 1804080.
27 E. Hajiesmaili and D. R. Clarke, *Journal of Applied Physics*, 2021, **129**, 151102.
28 L. Schertel, L. Siedentop, J. Meijer, P. Keim, C. M. Aegerter, G. J. Aubry and G. Maret, *Advanced Optical Materials*, 2019, **7**, 1900442.
29 G. Shang, M. Eich and A. Petrov, *APL Photonics*, 2020, **5**, 060901.
30 V. Hwang, A. B. Stephenson, S. Barkley, S. Brandt, M. Xiao, J. Aizenberg and V. N. Manoharan, *Proc Natl Acad Sci USA*, 2021, **118**, e2015551118.
31 M. Xiao, A. B. Stephenson, A. Neophytou, V. Hwang, D. Chakrabarti and V. N. Manoharan, *Opt. Express*, 2021, **29**, 21212–21224.
32 G. H. Lee, J. B. Kim, T. M. Choi, J. M. Lee and S.-H. Kim, *Small*, 2019, **15**, 1804548.
33 H. Stoyanov, D. Mc Carthy, M. Kollosche and G. Kofod, *Applied Physics Letters*, 2009, **94**, 232905.
34 Z. Wu, *Science*, 2004, **305**, 1273–1276.
35 G. Sharma and R. Bala, *Digital color imaging handbook*, CRC press, 2017.
36 H. Zhao, A. M. Hussain, M. Duduta, D. M. Vogt, R. J. Wood and D. R. Clarke, *Advanced Functional Materials*, 2018, **28**, 1804328.
37 Z. Wang, X. Jia, P. Zhang, Y. Liu, H. Qi, P. Zhang, U. Kaiser, S. Reineke, R. Dong and X. Feng, *Advanced Materials*, 2021, 2106073.
38 K. Madasamy, D. Velayutham, V. Suryanarayanan, M. Kathiresan and K.-C. Ho, *Journal of Materials Chemistry C*, 2019, **7**, 4622–4637.
39 C. Liu, Z. Fan, Y. Tan, F. Fan and H. Xu, *Advanced Materials*, 2020, **32**, 1907569.

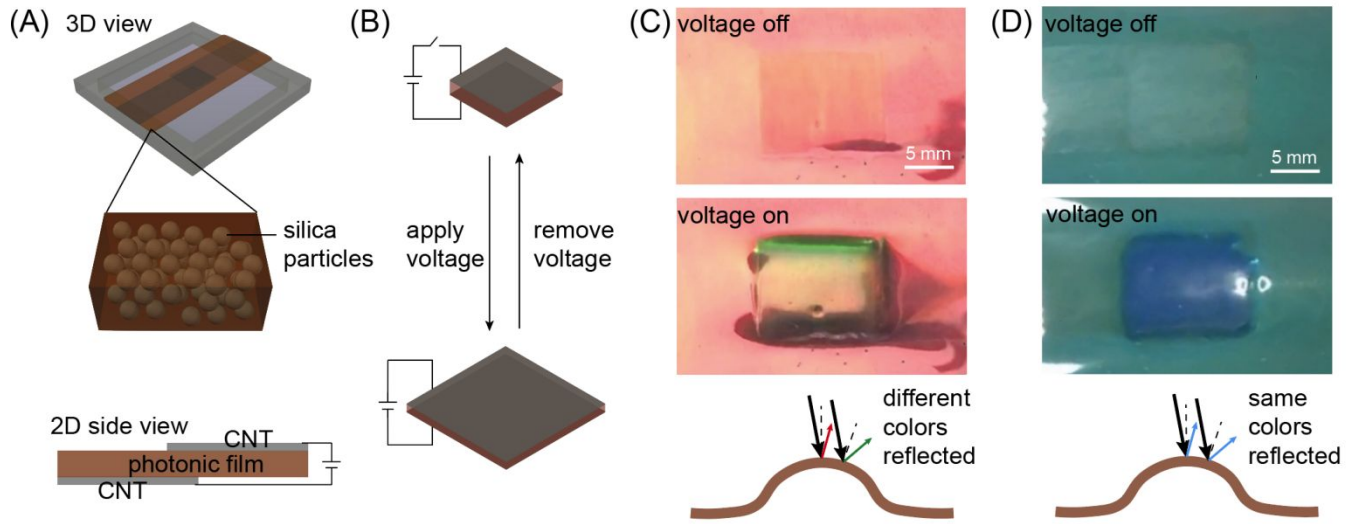

Figure 1. Comparison between crystalline and glassy dielectric elastomer films when actuated by the voltage. (A) 3D and 2D side-view diagrams of a photonic dielectric film used for voltage actuation. (B) Diagram showing how the elastomer sandwiched between CNT electrodes expands in area and reduces in thickness as the voltage is applied. Upon removal of the voltages, the elastomer returns to its initial dimensions. Images of crystalline (C) and glassy (D) films when the voltage is on (1.7 kV) and off. Both films have electrode areas of 13 mm × 10 mm and the thickness is 125 μm. The crystalline composite film contains monodisperse silica nanoparticles with a mean diameter of 224 $\pm$ 11 nm; and the glassy composite film contains a mixture of silica nanoparticles with mean diameters of 197 nm and 168 nm with volume ratio of 80:20 (overall number-average diameter of 190 $\pm$ 14 nm; see diameter histogram in Figure S1).

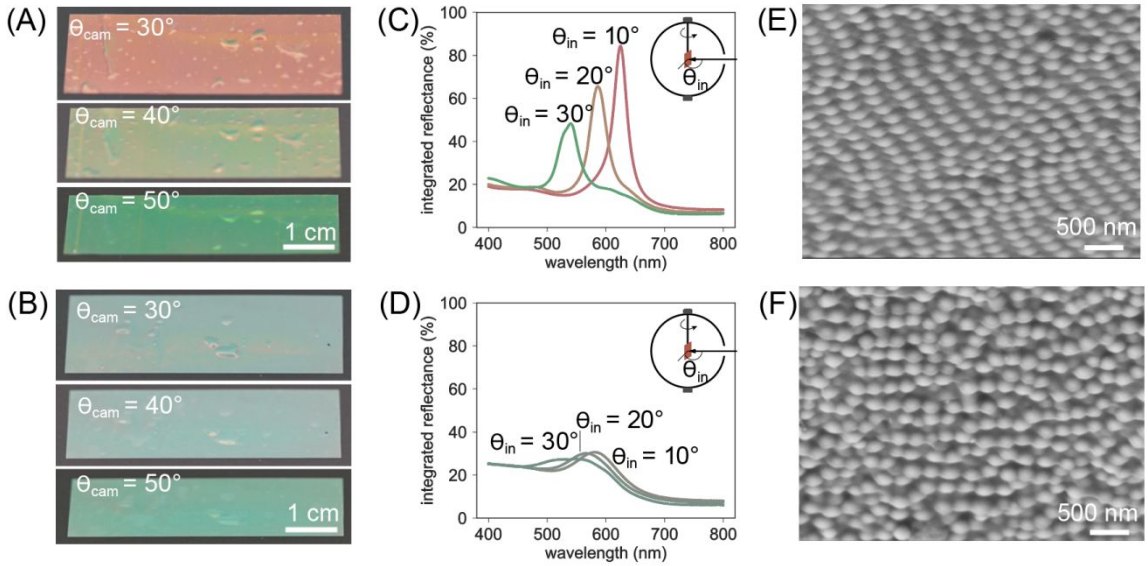

Figure 2. Optical properties and nanostructures of crystalline and glassy photonic films. Optical properties and nanostructures of the crystalline film (monodisperse 204 nm silica particles) and the glassy sample (binary 204 nm/164 nm silica nanoparticles) elastomers. (A-B) Photographs of the crystalline and glassy films taken in a light box with the camera placed at three different angles, 30°, 40°, and 50°, showing that the glassy film has much less angle-dependence. (C-D) Reflectance of the crystalline and glassy films measured by an integrating sphere at three different incident angles. The colors of the curves approximate the color perceived by the human eye for each reflectance spectrum, based on calculations using the CIELAB color space. (E-F) Cross-sectional SEM images of the crystalline and glassy films. The crystalline film is made of monodisperse silica particles with diameter 204 ± 7 nm (see diameter histogram in Figure S13A) and the glassy film is doped with 20% secondary silica particles with diameter 164 ± 13 nm (diameter histogram in Figure S13B).

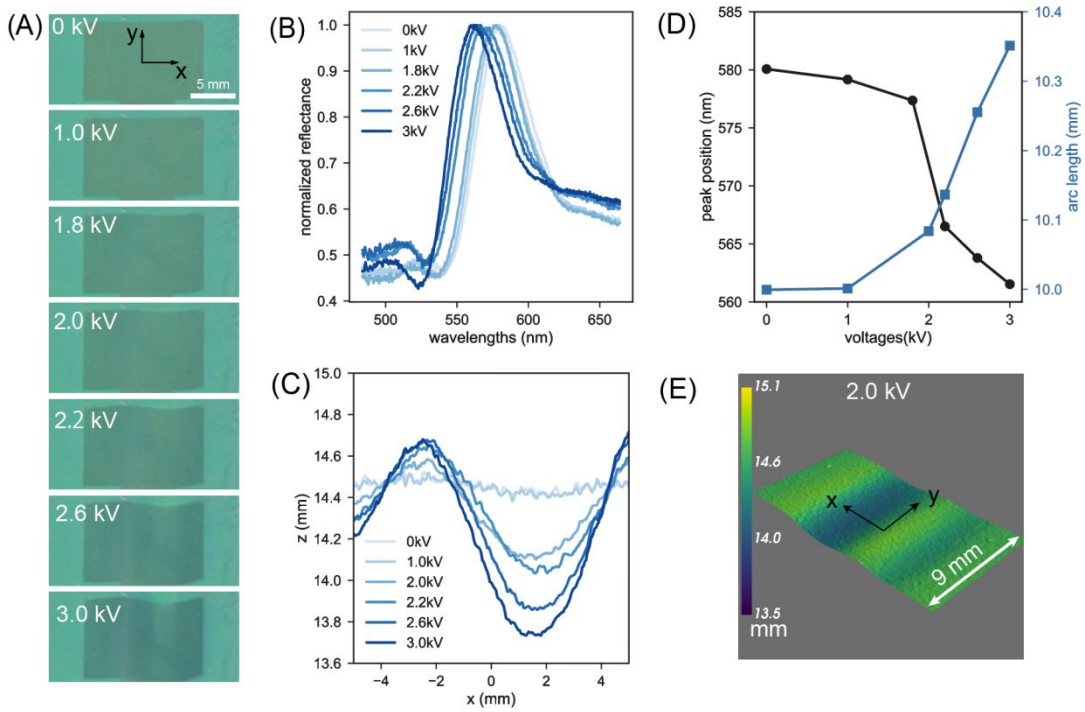

Figure 3. Quantification of color changes and deformation under a series of voltages. (A) Photographs of a glassy sample under different voltages, taken in a light box with a camera angle of 40°. (B) Normalized reflectance spectra with normal incident illumination measured by fiber-optic-based spectrometer attached to a microscope. (C) Height plots along *y* direction under different voltages. (D) Plot of the changes in peak positions and length of deformed area along *y* direction as a function of voltages. (E) 2D height profile for a glassy film subject to 2.0 kV.

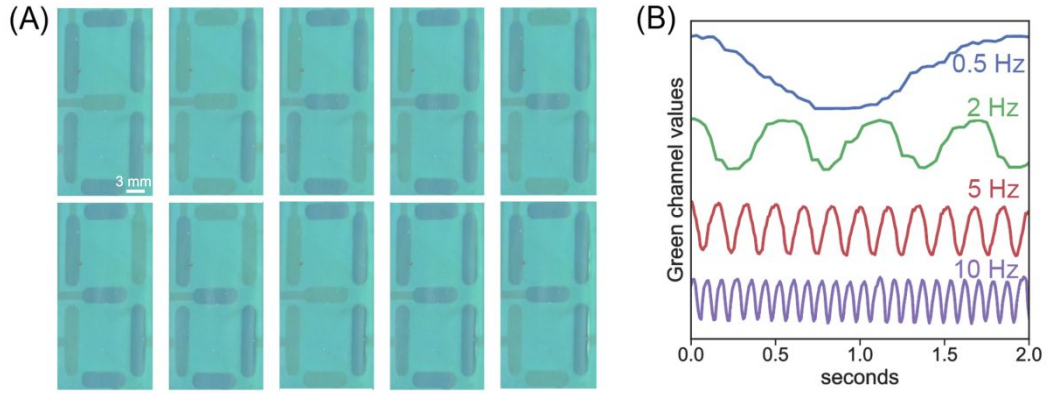

Figure 4. Pixelated color display made by a glassy elastomer composite. (A) Photographs of the display showing Arabic numerals from 0 up to 9 under a voltage of 2.0 kV (see also Movie S7). (B) Changes of the colors at different frequencies. We plot the green channel values of the RGB-encoded frames as a function of time to quantify the color change. The sample contains binary silica particles (binary 204 nm/164 nm with volume mixing ratio of 40:60). The film thickness is 125 μm before any pre-stretch.